A&A 444, 831–836 (2005)
DOI: 10.1051/0004-6361:20053700

Astronomy & Astrophysics

Star cluster detection with WFC/ACS in M 33⋆,⋆⋆

33 new clusters and 51 candidates

L. R. Bedin[1], G. Piotto[2], G. Baume[2,3], Y. Momany[2], G. Carraro[2,4], J. Anderson[5], M. Messineo[1], and S. Ortolani[2]

[1] European Southern Observatory, Karl-Schwarzschild-Str. 2, 85748, Garching, Germany
e-mail: lbedin@eso.org
[2] Dipartimento di Astronomia, Università di Padova, vicolo dell'Osservatorio 2, Padova 35122, Italy
e-mail: [piotto,momany,ortolani]@pd.astro.it
[3] Facultad de Ciencias Astronómicas y Geofísicas de la UNLP, IALP-CONICET, Paseo del Bosque s/n, La Plata, Argentina
e-mail: gbaume@fcaglp.fcaglp.unlp.edu.ar
[4] Andes Fellow, Departamento de Astronómia, Universidad de Chile, Casilla 36-D, Santiago, Chile
e-mail: gcarraro@das.uchile.cl
[5] Department of Physics and Astronomy, Mail Stop 108, Rice University, 6100 Main Street, Houston, TX 77005, USA
e-mail: jay@eeyore.rice.edu

Received 27 June 2005 / Accepted 19 August 2005

ABSTRACT

In this work we present the detection of 33 star clusters and 51 candidates in one field of the near by galaxy M 33. This study is based on WFC/ACS images available from the *HST* archive. Thanks to the high resolving power, we were able to confirm that two candidates previously indicated by Christian & Schommer (1982, ApJS, 49, 405) are indeed star clusters. We list the main properties for the star clusters (and candidates), along with some peculiar objects, such as background galaxies and possible HII regions.

Key words. catalogs – galaxies: clusters: general

1. Introduction

The distribution and properties of star clusters provide fundamental information for understanding star-formation history within galaxies, and how it is related to the dynamical and to the chemical enrichment history of the system.

The face-on orientation of Scd-galaxy M 33 minimizes absorption effects and makes it an ideal target for studying cluster distributions in spiral galaxies. Moreover, it has a morphology intermediate between the large spiral galaxies and the dwarf irregulars of our Local Group. Finally, it is close enough to make identifying star clusters almost straightforward on images collected from space with *HST*.

M 33's star clusters have been the subject of several studies from the ground in the recent past (Hiltner 1960; Kron & Mayall 1960; Melnick & D'Odorico 1978; Christian & Schommer 1982, 1988), and, with more success, from space (Chandar et al. 1999a, 2001). The last two works based on 55 WFPC2/HST fields, discovered 162 candidate star clusters. Here we present a new list of 33 candidate open clusters, discovered on a single ACS/HST WFC field. Even if we are limited to just one $\sim 3' \times 3'$ field, we were able to increase the number of known star clusters in M 33 by 20% with respect to previous works based on WFPC2 images, is the result of the superb resolving capabilities and sensitivity of the WFC/ACS.

The purpose of this paper is to continue the ongoing mapping of the M 33's star cluster population, with the aim of exploring the faintest part of the cluster distribution. These clusters would be excellent targets for multicolor or spectroscopic follow-up to measure cluster parameters, such as age.

2. Data and reduction

Proposals GO-9480/9578 (PI: Rhodes) took several parallel fields with the purpose of studying the amount and the distribution of dark matter, which, with its gravity, causes small distortions in the shapes of background galaxies.

One of these parallel fields falls in M 33, and it is the source of the present work. The field is centered at $(\alpha, \delta) = (1^{\rm h}34^{\rm m}02^{\rm s}, 30°48'46'')$, with a position angle of the *HST* V3-axis of $\sim 70°$. The data set includes 5 images in *F775W* band (SDSS-*i*), one

⋆ Based on observations with the NASA/ESA *Hubble Space Telescope*, obtained at the Space Telescope Science Institute, which is operated by AURA, Inc., under NASA contract NAS 5-26555.
⋆⋆ Figures 1–3 are only available in electronic form at http://www.edpsciences.org

Table 1. Catalog of the newly identified clusters in the ACS/WFC studied field. This table gives the main properties.

ID	$(\alpha)_{J2000}$	$(\delta)_{J2000}$	Radius″	$\int m_{F775W}$	Remarks
001	01:34:07.0	+30:50:57.3	3.0, 3.0, 1.17 ± 0.64	17.30 ± 0.40	compact
002	01:34:07.5	+30:50:10.8	2.0, 2.0, 1.09 ± 0.58	17.67 ± 0.10	compact
					U1200_00651686, N33013119190
003	01:34:06.6	+30:50:18.1	1.0, 1.0, 0.82 ± 0.48	18.54 ± 0.10	compact
					U1200_00651580, N33013119228
004	01:34:05.8	+30:49:56.8	2.0, 2.0, 1.14 ± 0.57	17.03 ± 0.10	compact
					U1200_00651484, N33013119151
					HII region # H 8, in CS82
005	01:34:05.1	+30:49:42.7	2.0, 2.0, 0.63 ± 0.44	17.73 ± 0.40	low density
					N33013118960
006	01:34:07.3	+30:47:41.8	2.0, 2.0, 0.64 ± 0.57	17.62 ± 0.10	low density
007	01:34:03.9	+30:47:29.1	5.0, 6.0, 1.26 ± 0.70	15.52 ± 0.20	populous
					U1200_00651247
008	01:34:06.7	+30:48:56.2	2.0, 2.0, 1.23 ± 9.14	17.26 ± 0.10	low density + HII
					U1200_00651585, N33013118554
009	01:34:06.7	+30:48:32.7	3.0, 1.0, 0.89 ± 0.44	16.97 ± 0.35	compact
					U1200_00651589, N33013118415
010	01:34:03.1	+30:48:11.1	3.0, 1.5, 0.83 ± 0.69	17.26 ± 0.40	compact
011	01:34:08.7	+30:48:14.6	1.5, 1.0, 0.60 ± 0.61	18.29 ± 0.35	low density
012	01:34:05.4	+30:47:50.9	6.0, 6.0, ?	15.21 ± 0.10	association
					U1200_00651432
013	01:34:02.7	+30:48:36.8	1.5, 1.5, 1.19 ± 5.04	17.65 ± 0.20	low density
					N33013118386
014	01:34:02.3	+30:50:27.6	1.5, 1.5, 1.46 ± 1.47	18.25 ± 0.15	populous
					U1200_00651038, N33013119312
015	01:34:02.6	+30:48:30.6	3.0, 3.0, 1.65 ± 3.00	17.46 ± 0.35	low density
016	01:34:06.8	+30:47:26.2	2.0, 2.0, 2.21 ± 4.14	16.31 ± 0.10	populous
017	01:34:04.8	+30:47:39.1	10.0, 10.0, ?	14.38 ± 0.25	association
018	01:33:56.9	+30:49:26.7	2.0, 2.0, 1.06 ± 1.86	17.33 ± 0.10	low density
					U1200_00650366, N33013118811
019	01:33:58.9	+30:49:10.7	?, 3.0, ?	16.65 ± 0.10	low density + HII
					U1200_00650604 N33013118699
020	01:33:57.8	+30:49:04.5	1.0, 1.0, 0.13 ± 6.00	18.74 ± 0.15	low density + HII
					N33013118702
021	01:33:58.5	+30:48:42.6	2.0, 2.0, 1.14 ± 4.26	17.51 ± 0.15	low density + HII
					N33013118700
022	01:34:00.2	+30:48:36.5	3.0, 2.0, 1.44 ± 1.31	16.91 ± 0.35	low density
					N33013118417
					cluster candidate # 42, in CS82
023	01:33:57.0	+30:48:03.4	2.0, 2.0, 0.79 ± 0.51	17.44 ± 0.10	low density
					N33013118121
024	01:33:54.7	+30:48:43.6	1.0, 2.0, 0.55 ± 0.54	18.37 ± 0.10	populous
					cluster candidate # 41, in CS82
025	01:34:01.6	+30:49:44.0	3.0, 3.0, 1.49 ± 0.68	16.59 ± 0.15	populous
					U1200_00650971 N33013118963
					HII region # H 9, in CS82
026	01:34:00.7	+30:50:08.7	?, 2.0, 2.44 ± 4.45	17.37 ± 0.20	low density
					U1200_00650842 N33013119201
027	01:34:04.7	+30:49:17.8	?, 2.0, ?	17.34 ± 0.10	low density
					U1200_00651350, N33013118734
028	01:33:59.4	+30:47:29.7	2.0, 2.0, 1.01 ± 1.10	17.69 ± 0.10	compact
029	01:33:59.6	+30:47:38.3	2.0, 1.0, 0.24 ± 0.29	17.90 ± 0.15	low density
030	01:34:01.0	+30:46:58.7	2.0, 2.0, 0.10 ± 1.95	17.63 ± 0.10	compact
031	01:33:59.0	+30:50:05.8	2.0, 2.0, 0.37 ± 0.12	17.45 ± 0.20	populous
					N33013119141
032	01:33:59.4	+30:48:26.7	2.0, 1.0, 0.56 ± 0.63	18.04 ± 0.20	low density
033	01:34:07.0	+30:49:24.4	2.0, 1.0, 0.90 ± 0.41	17.23 ± 0.10	compact
					U1200_00651624, N33013118796

of 400 s, and four of 700 s. Figure 1 shows that our ACS field is located between two spiral arms of M 33, partially overlapping the arms themselves.

We stacked the five FLT images into a distortion-corrected super-sampled frame using the distortion correction of Anderson (2002) and the stacking technique described in King et al. (2005). Briefly, we determined the corresponding location in each of the FLT images for each pixel in the super-sampled image. We then interpolated the five FLT images at this location to get five estimates for the pixel value at the stacked-frame location. We then used a sigma-clipped mean to arrive at a value for each pixel in the super-sampled frame. This image of 9000 × 9000 pixels, with a pixel scale of 25 mas/pixel, can be download from the web-site: `http://www.eso.org/~lbedin/M33/M33.fits.gz` (~68 Mb).

The astrometric calibration of the M 33 reference image was computed employing stars from the GSC2.2 catalog and using the IRAF MSCRED package (Valdes 1998). Of the ~100 GSC2.2 stars, we extracted and used only 12 "good" stars that seemed associated with resolved stars. The rest of GSC2.2 were clearly unresolved objects. The external accuracy (absolute astrometry) was estimated to be about 0.30 arcsec. This was made comparing the rms of the GMS2.2 catalog with the positions of the same objects measured in our image (whose header contains the WCS informations of our astrometric solution). The internal precision (relative astrometry) is much higher than that, better than one mas (Anderson 2002; Anderson et al. 2005 in preparation).

The fluxes measured on this image were calibrated to the Vega-mag WFC/ACS system described in Bedin et al. (2005), which is consistent with Sirianni et al. (2005).

3. The catalog

In Figs. 2 and 3 we show the location of the 33 new star-cluster candidates identified in our field. The WFC/ACS field overlaps neither with any of the WFPC2 fields in Chandar et al. (1999a–c) and of Chandar et al. (2001) nor with any of the CCD fields in Christian & Schommer (1988), but it does contain two cluster candidates and two HII regions indicated by Christian & Schommer (1982, hereafter CS82) on a photographic plate-based study.

We did not need to develop a special algorithm to detect star clusters. On ACS images at the distance of M 33, most of the star clusters can be detected by eye on the super-stack image on which, assuming a distance of 840 kpc for M 33 (Freedman et al. 1991), one pixel (0.″025) corresponds to 0.1 pc (i.e. one parsec is mapped by 10 pixels).

Table 1 lists our new candidate star clusters. The first three columns give the ID number and the (α, δ) position at J2000.0; Col. 4 gives radius, and Col. 5 the integrated *F775W* magnitude ($\int m_{F775W}$). Some clusters were identified as a star in the GSC-2 and/or USNO catalog, so we also listed their corresponding identification numbers in Col. 6.

To derive clusters radius, we built their individual radial profiles by using three methods. The first one is the standard "star counts method" within 0.5 arcsec wide concentric annuli, previous star detections, and PSF photometry for each cluster.

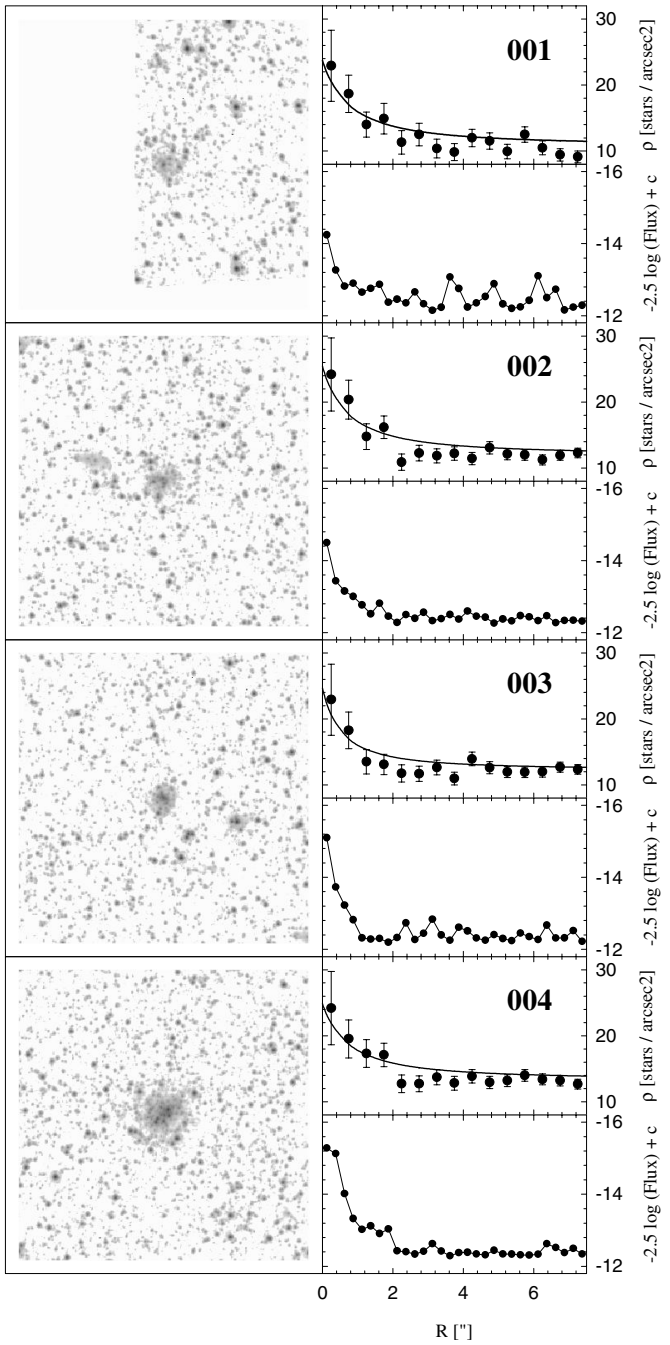

Fig. 4. Example of radius determination for the first four clusters in the catalog presented in this work. For each cluster, the radius was obtained with three different methods (see the text).

The second method directly employed the measure of the flux, say −2.5×log (counts/area), within 0.25 arcsec wide concentric annuli. The third method made use of the formalism developed by Mackey & Gilmore (2003) to derive an estimate of the radius of a star cluster. The fitting formula (Eq. (3) in their paper) reads:

$$\mu = \mu_0 \times (1 + (r/a)^2)^{(-\gamma/2)} + \phi,$$

where μ is the stellar density and r the distance from the cluster center. We calculated ϕ as the average stellar density at $3.5 \leq r[\text{arcsec}] \leq r = 7.0$. Finally, γ is always kept below 3.

Table 2. Bright galaxies and miscellaneous objects.

ID	$(\alpha)_{J2000}$	$(\delta)_{J2000}$	Radius″	$\int m_{F775W}$	Remarks
034	01:34:06.7	+30:47:27.8	16.	13.30 ± 0.4	HII, shell structure
035	01:34:10.3	+30:48:40.9	2.0	18.02 ± 0.2	background galaxy
036	01:34:08.5	+30:49:20.3	2.1	17.74 ± 0.1	background galaxy
037	01:34:09.2	+30:49:35.0	1.9	18.16 ± 0.1	background galaxy
038	01:34:09.2	+30:48:48.7	2.5	17.59 ± 0.1	background galaxy
039	01:34:09.2	+30:47:54.1	1.5	18.57 ± 0.2	background galaxy
040	01:34:10.0	+30:47:49.5	1.8	18.04 ± 0.3	background galaxy
041	01:33:56.9	+30:49:24.0	2.7	17.14 ± 0.3	background galaxy
042	01:33:56.2	+30:49:17.1	1.6	18.47 ± 0.2	background galaxy
043	01:33:55.0	+30:48:53.2	2.5	17.62 ± 0.2	background galaxy
044	01:33:55.3	+30:49:53.6	1.8	18.31 ± 0.3	background galaxy
045	01:34:02.1	+30:49:54.4	4.0	16.42 ± 0.2	background galaxy
046	01:33:59.9	+30:50:10.5	2.1	17.93 ± 0.3	background galaxy
047	01:34:03.6	+30:49:47.7	3.4	16.88 ± 0.2	background galaxy
048	01:34:03.9	+30:49:55.4	1.4	18.95 ± 0.4	background galaxy
049	01:34:02.8	+30:49:40.9	2.6	17.40 ± 0.4	background galaxy
050	01:34:03.2	+30:49:44.3	1.7	18.24 ± 0.2	background galaxy
051	01:33:58.8	+30:50:04.3	5.0	15.88 ± 0.1	background galaxy
052	01:33:58.4	+30:50:03.2	0.9	19.60 ± 0.2	background galaxy
053	01:33:53.7	+30:49:41.4	0.6	20.16 ± 0.2	background galaxy
054	01:33:56.6	+30:49:23.9	1.6	18.50 ± 0.2	background galaxy
055	01:34:01.6	+30:48:29.1	2.0	17.97 ± 0.2	background galaxy
056	01:33:56.2	+30:48:25.8	1.3	18.64 ± 0.2	background galaxy N33013118306
057	01:33:59.5	+30:47:23.6	1.6	18.24 ± 0.3	HII

The three methods applied to all the clusters and candidates, and the corresponding values (when available) reported in Col. 4. As for the fitting, we only report the derived radius (a) with the corresponding error. As an example, in Fig. 4 we show the derived profiles for the first four clusters of our catalog and the corresponding fits. In some cases, however, the fit with the Mackey & Gilmore formula was not possible due to the complicated structure of the profile. For these cases, a question mark is inserted.

Notice that in almost all the cases, the three determinations are very similar within the errors. Because of its definition of core radius (Mackey & Gilmore 2003), the values of a are always smaller than the other two radius estimates, which were derived as the distances from the cluster center at which the stellar profile reaches the background.

The integrated magnitude obtained as the integral of the flux within the indicated radius. The related uncertainties obtained from the rms of the background fluxes from 4 areas of equal size around the cluster candidate center. These uncertainties do not take uncertainties in the cluster radius into account. The flux calibrated to the Vega-mag system. Furthermore, Col. 6 associates a simple morphological description to each cluster based on their size and degree of concentration. Those clusters with higher central concentration and approximately spherical symmetry are classified as *compact*; the others as *low density*. The clusters richest in stars have been labeled as *populous*, and wide groups of bright stars are considered as probable *associations*.

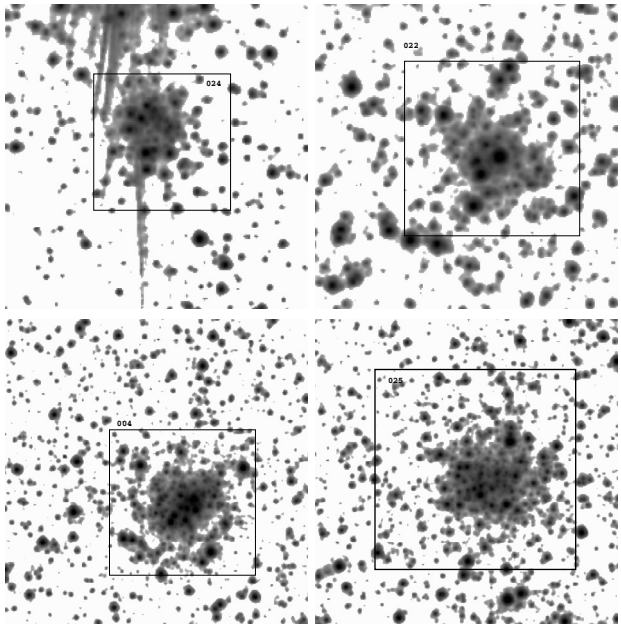

Fig. 5. (*Top panels*) The two cluster candidates labeled in CS82 as #41 and #42, were confirmed in this work to be star clusters; namely: 24, 22 according to IDs given in Table 1. (*Bottom panels*) Also, the two HII regions labeled in CS82 as H#8 and H#9 were confirmed in this work to be star clusters, whose IDs are 4, 25, respectively.

The transmission curve for the *F775W* filter includes several emission lines that are commonly seen in HII regions

Table 3. Other cluster candidates.

ID	$(\alpha)_{J2000}$	$(\delta)_{J2000}$	Radius″	$\int m_{F775W}$	Remarks
058	01:34:06.7	+30:50:41.7	?, 1.5, ?	18.66 ± 0.25	low density
059	01:34:07.3	+30:50:13.6	2.0, 1.0, ?	18.54 ± 0.20	low density + HII
060	01:34:06.3	+30:50:42.3	1.0, 2.0, 0.57 ± 2.26	18.45 ± 0.20	low density
061	01:34:09.5	+30:48:30.1	1.5, 1.0, 1.96 ± 3.63	19.03 ± 0.15	low density
062	01:34:09.2	+30:48:25.5	2.0, 1.0, 1.61 ± 5.77	18.22 ± 0.10	low density
063	01:34:06.9	+30:47:54.0	2.0, 2.0, ?	17.70 ± 0.25	low density, N33013118144
064	01:34:05.3	+30:49:06.5	2.0, 1.0, 0.29 ± 0.22	18.47 ± 0.20	low density
065	01:34:03.6	+30:50:32.0	3.0, 2.0, 0.76 ± 0.47	17.56 ± 0.45	low density
066	01:34:04.1	+30:50:22.2	3.0, 2.0, 0.61 ± 0.71	17.50 ± 0.10	compact
067	01:34:04.8	+30:50:36.2	2.0, 2.0, 0.64 ± 0.53	17.58 ± 0.15	low density
068	01:34:04.8	+30:50:27.5	1.0, 2.0, ?	18.01 ± 0.25	low density
069	01:34:06.6	+30:50:52.9	4.0, 3.0, ?	16.51 ± 0.15	low density, U1200_00651686
070	01:34:08.8	+30:48:41.2	2.0, 1.0, 0.92 ± 0.61	17.67 ± 0.10	low density
071	01:34:08.1	+30:48:13.9	2.0, 1.0, ?	17.93 ± 0.10	low density
072	01:34:10.9	+30:48:06.1	2.0, 2.0, 0.08 ± 8.97	17.82 ± 0.15	low density
073	01:34:10.3	+30:48:00.1	1.0, 2.0, 0.12 ± 2.95	18.35 ± 0.40	low density
074	01:34:03.3	+30:49:03.6	2.0, 2.0, 0.32 ± 0.37	17.69 ± 0.15	compact, N33013118634
075	01:34:02.8	+30:48:59.7	2.0, 2.0, 1.55 ± 1.22	17.91 ± 0.20	low density, N330131127966
076	01:34:04.2	+30:48:19.8	2.0, 1.5, 0.16 ± 5.68	18.26 ± 0.35	low density
077	01:34:06.7	+30:47:44.5	1.0, 1.0, 0.21 ± 1.64	19.22 ± 0.20	low density
078	01:34:06.9	+30:47:37.1	1.5, 1.5, ?	18.08 ± 0.15	low density
079	01:34:06.7	+30:47:34.2	1.0, 1.5, 0.10 ± 3.83	18.15 ± 0.15	low density
080	01:34:06.9	+30:47:32.6	1.0, 1.0, ?	19.06 ± 0.15	low density
081	01:34:06.0	+30:47:29.6	2.0, 2.0, 0.15 ± 3.64	17.40 ± 0.15	low density + HII
082	01:34:06.8	+30:47:22.5	1.5, 2.0, ?	17.05 ± 0.20	low density + HII
083	01:33:57.9	+30:49:32.5	2.0, 2.0, 0.71 ± 0.54	17.93 ± 0.30	low density
084	01:33:56.8	+30:49:04.8	4.0, 4.0, 2.44 ± 1.89	16.57 ± 0.15	low density association, N33013118619
085	01:33:58.4	+30:48:33.0	2.0, 1.0, ?	18.38 ± 0.15	low density, N33013118704
086	01:33:58.7	+30:48:47.3	2.0, 2.0, 0.06 ± 1.21	17.79 ± 0.15	low density
087	01:33:57.3	+30:48:41.1	3.0, 3.0, 1.01 ± 0.77	17.09 ± 0.25	low density
088	01:34:01.4	+30:47:47.0	1.5, 2.0, 0.94 ± 1.22	18.18 ± 0.10	low density, N33013118121
089	01:33:54.3	+30:49:16.7	1.5, 2.0, 0.80 ± 0.42	18.13 ± 0.15	compact
090	01:33:53.7	+30:49:14.6	2.0, 2.0, 0.63 ± 1.03	17.93 ± 0.25	low density
091	01:33:57.6	+30:48:51.7	2.0, 2.0, 0.13 ± 3.65	17.84 ± 0.30	low density
092	01:33:58.9	+30:48:49.0	60., ?, ?	10.59 ± 0.30	association
093	01:34:00.7	+30:50:13.8	2.0, 2.0, 0.67 ± 1.15	17.73 ± 0.15	compact
094	01:34:02.3	+30:50:08.7	2.0, 2.5, 0.15 ± 3.42	17.70 ± 0.15	low density
095	01:34:01.7	+30:50:07.1	3.0, 2.0, 2.31 ± 3.71	17.54 ± 0.50	low density
096	01:33:59.2	+30:46:50.5	2.0, 3.0, 0.14 ± 3.74	17.05 ± 0.15	low density
097	01:33:59.3	+30:47:11.4	3.0, 2.0, 1.04 ± 1.17	17.34 ± 0.15	low density
098	01:34:01.2	+30:46:52.5	3.0, 2.0, 0.90 ± 2.44	17.42 ± 0.55	low density
099	01:34:00.3	+30:47:59.9	2.0, 2.0, 0.99 ± 1.16	17.92 ± 0.25	compact
100	01:33:57.2	+30:46:47.1	2.5, 2.0, 0.15 ± 0.76	17.41 ± 0.35	compact
101	01:34:03.2	+30:50:05.5	1.0, 1.0, 0.06 ± 5.55	19.28 ± 0.20	low density, N330131127965
102	01:34:05.7	+30:50:30.0	1.5, 1.0, ?	19.12 ± 0.10	compact
103	01:34:01.5	+30:49:33.2	2.0, 2.0, 0.19 ± 1.62	18.03 ± 0.35	low density
104	01:33:59.2	+30:48:38.9	2.5, 1.5, 0.34 ± 0.24	17.99 ± 0.25	compact
105	01:33:58.7	+30:49:23.7	1.5, 1.0, 0.27 ± 2.08	18.88 ± 0.35	compact
106	01:33:59.8	+30:49:21.4	1.5, 2.0, ?	18.17 ± 0.15	low density + HII
107	01:33:57.5	+30:49:07.5	3.0, 2.0, 0.46 ± 0.42	17.42 ± 0.20	low density
108	01:33:59.9	+30:48:27.8	?, 1.8, ?	18.18 ± 0.15	low density
109	01:33:58.9	+30:47:45.3	1.5, 2.0, 0.10 ± 7.13	17.95 ± 0.20	low density
110	01:34:05.1	+30:50:39.7	2.0, 2.0, 0.10 ± 1.43	17.76 ± 0.25	low density

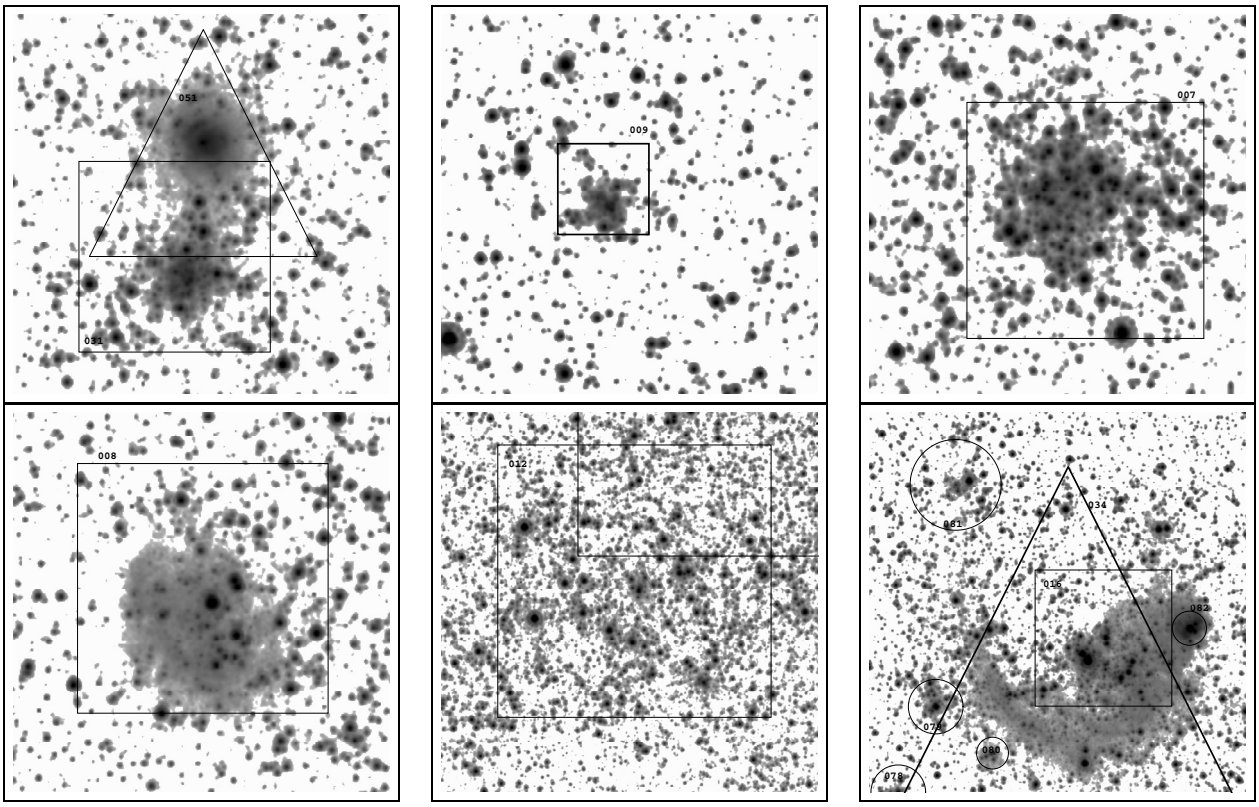

Fig. 6. Example of galaxy (51), populous cluster (31), compact (9), populous (7), low density + HII(8), association (12), and HII shell structure (34).

– HeI(7065), ArIII(7136), HeI(7282), OII(7321), ArIII(7752), HI(8359), HI(8374), HI(8392), HI(8413), HI(8437), OI (8446), HI(8467), HI(8502) – of which the strongest typically is ArIII(7136) with an intensity of 10−20 times that of the H_β line (Esteban et al. 2002; Lee & Skillman 2004). We therefore identified as HII all those objects which show faint diffuse brightness, but we do not distinguish between SN remnants and star-formation regions. In Table 2 we list some background bright galaxy candidates and two other notable objects. Table 3 contains a list of diffuse objects which could be either low density star cluster candidates or HII regions; see Fig. 6 for examples of this morphological classification.

4. Conclusion and the future

The HST archive continues to serve as a gold mine full of secondary science. In this work, we used an ACS/HST parallel field taken for other purposes to identify 33 star cluster candidates in the spiral galaxy M 33. We were able to confirm 2 cluster candidates previously suggested by CS82 and to reveal two objects classified as HII regions in the same work, each hosting a star cluster (Fig. 5). We give the size and a preliminary photometry both for these clusters and for an additional 51 objects that are less certain to be clusters.

Follow-up multi-band observations or spectroscopy could provide additional cluster parameters, such as color and age.

Acknowledgements. We thank the anonymous referee for careful reading of the manuscript and for the useful suggestions. We acknowledge the support of the Italian MIUR under the program PRIN2003. The work of GC was supported by *Fundación Andes*.

References

Anderson, J. 2002, HST Calibration Workshop 2002, ed. S. Arribas, A. Koekemoer, & B. Whitmore (Baltimore: STScI), 13
Bedin, L. R., et al. 2005, MNRAS, 357, 1038
Chandar, R., Bianchi, L., & Ford, H. C. 1999a, ApJS, 122, 431
Chandar, R., Bianchi, L., & Ford, H. C. 1999b, ApJ, 517, 668
Chandar, R., Bianchi, L., Ford, H. C., & Salasnich, B. 1999c, PASP, 111, 794
Chandar, R., Bianchi, L., & Ford, H. C. 2000, A&A, 336, 498
Christian, C. A., & Schommer, R. A. 1982, ApJS, 49, 405 [CS82]
Christian, C. A., & Schommer, R. A. 1988, AJ, 95, 704
Esteban, C., Peimbert, M., Torres-Peimbert, S., & Rodríguez, M. 2002, ApJ, 581, 241
Freedman, W. L., Wilson, C. D., & Madore, B. F. 1991, ApJ, 372, 455
Hiltner, W. A. 1960, ApJ, 131, 163
King, I. R., Bedin, L. R., Piotto, G., Cassisi, S., & Anderson, J. 2005, AJ, in press
Kron, G. E., & Mayall, G. U. 1960, AJ, 65, 581
Lee, H., & Skillman, E. D. 2004, ApJ, 614, 698
Mackey, A. D., & Gilmore, G. F. 2003, MNRAS, 338, 85
Mochejska, B. J., Kaluzny, J., Krockenberger, M., Sasselov, D. D., & Stanek, K. Z. 1998, Acta Astron., 48, 455
Melnick, J., & D'Odorico, S. 1978, A&AS, 34, 249
Valdes, F. G. 1998, ASP Conf. Ser. 145: Astronomical Data Analysis Software and Systems VII, 7, 53

Online Material

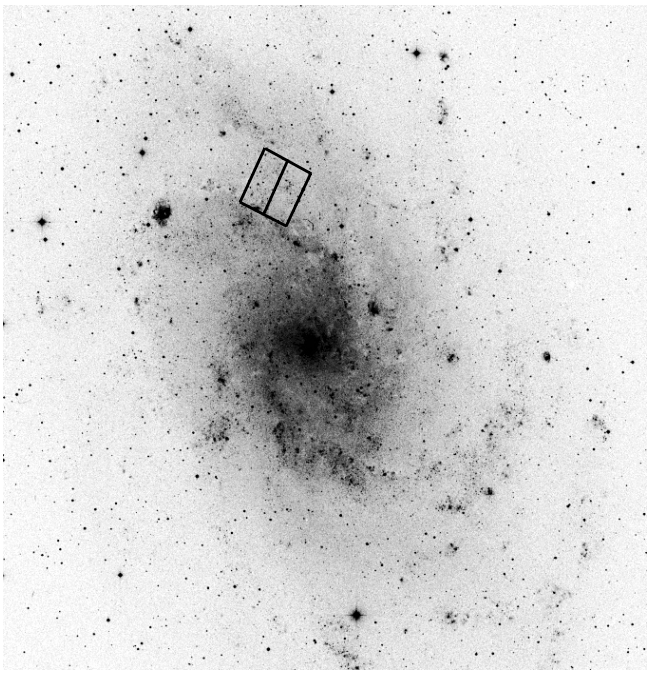

Fig. 1. WFC/ACS field finding chart. The field of view is $40' \times 40'$, North on top, and East to the left.

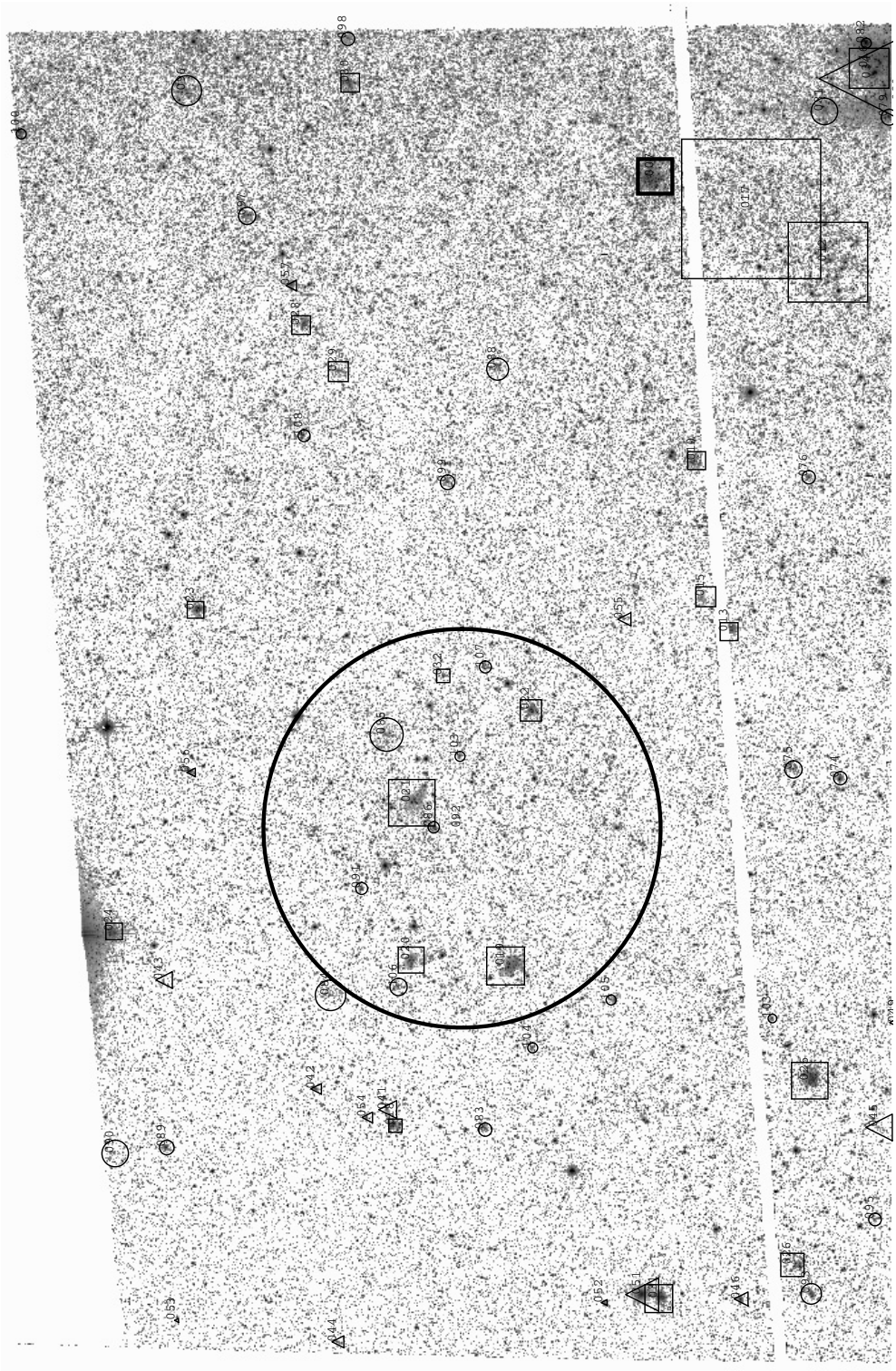

Fig. 2. Cluster identification charts for WFC/ACS top chip. Squares indicate the new clusters (Table 1), circles mark background galaxies (Table 2) and cluster candidates (Table 3). Triangles indicate the presence of gas or of diffuse objects.

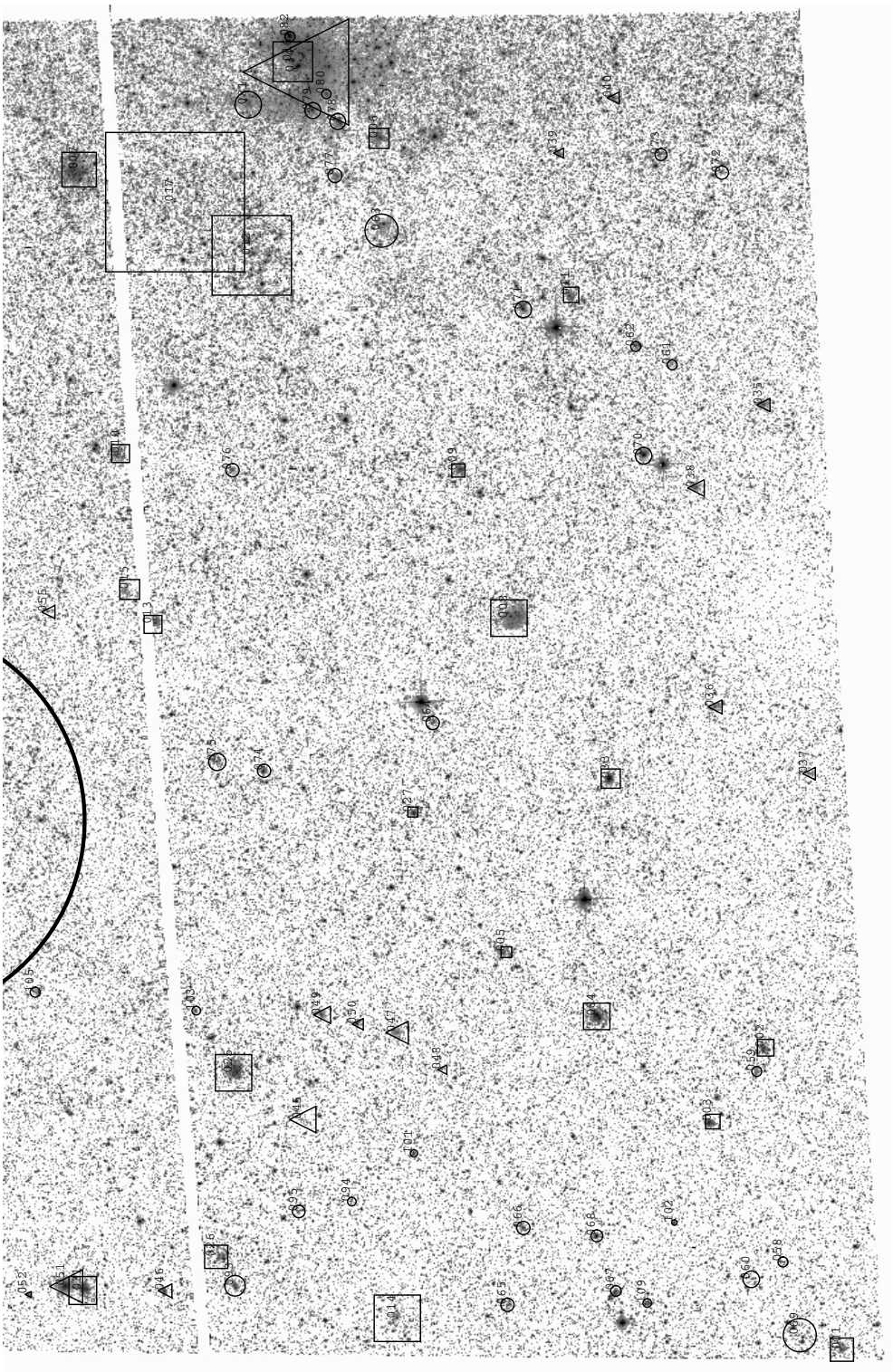

Fig. 3. Cluster identification charts for WFC/ACS bottom chip. Symbols as in Fig. 2.